


# Transplantation of Amniotic Fluid-Derived Stem Cells Preconditioned with Glial Cell Line-Derived Neurotrophic Factor Gene Alleviates Renal Fibrosis

Shulin Li<sup>1</sup>, Yuan Zhao<sup>1</sup>, Zhuojun Wang<sup>1</sup>, Jia Wang<sup>1</sup>,  
Caixia Liu<sup>1</sup>, and Dong Sun<sup>1,2</sup>

Cell Transplantation  
2019, Vol. 28(1) 65–78  
© The Author(s) 2018  
Article reuse guidelines:  
sagepub.com/journals-permissions  
DOI: 10.1177/0963689718815850  
journals.sagepub.com/home/ccl  


## Abstract

Amniotic fluid-derived stem cells (AFSCs), which exhibit both embryonic and mesenchymal stem cell characteristics, have been shown to mitigate the degree of renal interstitial fibrosis. The aim of the present study was to determine whether transplantation of glial cell line-derived neurotrophic factor (GDNF)-modified AFSCs is more useful than transplantation of unmodified AFSCs for the treatment of renal interstitial fibrosis. Mice were randomly assigned to a sham-operation group (sham), a unilateral ureteral obstruction (UUO)-saline solution group (UUO), an AFSC transplantation group (AFSC) and a GDNF-modified AFSC transplantation group (GDNF-AFSC) and sacrificed at days 3 and 7 post-surgery (six in each group). We showed that GDNF-AFSCs noticeably suppressed oxidative stress and inflammation; additionally, GDNF-AFSCs positively regulated peritubular capillaries (PTCs), vascular endothelial growth factor (VEGF), hypoxia inducible factor-1 $\alpha$  (HIF-1 $\alpha$ ), and transforming growth factor- $\beta$ 1 (TGF- $\beta$ 1) protein levels. Transmission electron microscopy (TEM) revealed that mitochondrial injury induced by the UUO model was significantly ameliorated after the mice were treated with GDNF-AFSCs. Therefore, we determined that GDNF gene promotes the abilities of AFSCs to inhibit inflammatory and oxidative stress effects, repair renal microvessels, relieve tissue hypoxia and mitochondrial damage, and, ultimately, alleviate renal interstitial fibrosis.

## Keywords

glial cell line-derived neurotrophic factor; amniotic fluid-derived stem cells; inflammation; oxidative stress; mitochondrial damage; renal interstitial fibrosis

## Introduction

Renal fibrosis, which is characterized by oxidative stress, chronic inflammation, massive interstitial myofibroblast activation, and excessive extracellular matrix (ECM) protein accumulation, is the final common pathway of virtually all types of progressive chronic kidney disease (CKD), ultimately leading to end-stage renal disease<sup>1–3</sup>. In the past decades, although many studies have been performed on potential treatments for suppressing CKD progression<sup>4,5</sup>, effective therapies are still limited owing to the incomplete understanding of the mechanisms underlying CKD. Oxidative stress and inflammation play crucial roles in renal fibrosis by regulating interstitial fibroblast proliferation, peritubular capillary injury, and microcirculatory impairment<sup>6</sup>. Increased concentrations of reactive oxygen species (ROS) are present in obstructed kidneys<sup>7</sup>, which cause

renal interstitial injury by lipid peroxidation, increased hydrogen peroxide levels, and DNA and protein damage<sup>8–10</sup>. Peritubular capillary (PTC) injury is secondary to oxidative stress and inflammation, which, in turn, results in chronic ischemia and hypoxia. Decreased renal oxygen

<sup>1</sup> Department of Nephrology, Affiliated Hospital of Xuzhou Medical University, Xuzhou, China

<sup>2</sup> Department of Internal Medicine and Diagnostics, Xuzhou Medical University, Xuzhou, China

Submitted: June 2, 2018. Revised: November 4, 2018. Accepted: November 6, 2018.

### Corresponding Author:

Dong Sun, Department of Nephrology, Affiliated Hospital of Xuzhou Medical University, 99 West Huai-hai Road, Xuzhou, Jiangsu, 221002, China.  
Email: sundong126@yahoo.com



Creative Commons Non Commercial CC BY-NC: This article is distributed under the terms of the Creative Commons Attribution-NonCommercial 4.0 License (<http://www.creativecommons.org/licenses/by-nc/4.0/>) which permits non-commercial use, reproduction and distribution of the work without further permission provided the original work is attributed as specified on the SAGE and Open Access pages (<https://us.sagepub.com/en-us/nam/open-access-at-sage>).

supply and tissue ischemia are common causes of mitochondrial damage and dysfunction<sup>11</sup>. Finally, mitochondrial damage and impaired homeostasis lead to bioenergetic dysfunction (reduced ATP generation), which cause mitochondrial ROS, lipid peroxidation, and apoptosis. Several studies have demonstrated that renal injury due to unilateral ureteral obstruction in rodents is associated with increased mitochondria-mediated renal tubular cell apoptosis, autophagy, and mitochondrial ROS<sup>12</sup>.

Among stem cell populations, embryonic stem cells are the most plastic and have indefinite self-renewal capacity. However, their application is limited by ethical and safety issues, while the clinical application of induced pluripotent stem cells is still limited because of their high teratogenicity potential<sup>13,14</sup>. Recent experiments have shown that amniotic fluid is a novel source of stem cells for therapeutic transplantation with no ethical and teratogenicity problems. Amniotic fluid-derived stem cells (AFSCs) can differentiate into cells of the three embryonic germ layers and express the transcription factor Oct-4, a marker of embryonic and mesenchymal stem cells<sup>15,16</sup>. In our previous study, we demonstrated that transplantation of AFSCs enhanced PTC repair, alleviated tissue hypoxia, and mitigated the degree of renal interstitial fibrosis<sup>14</sup>. Glial cell line-derived neurotrophic factor (GDNF), isolated as a neurotrophic factor for midbrain dopaminergic neurons, has long been considered as a main potential therapy for neuronal diseases<sup>17–19</sup>. However, Pichel et al. found that GDNF<sup>-/-</sup> mutant mice showed kidney agenesis and dysgenesis, which indicates that GDNF plays an important role in the development of renal system<sup>20,21</sup>. Meng et al. showed that the spermatogenic stem cells entered the differentiation pathway at a reduced dosage of GDNF; on the other hand, the stem cells could only self-renew but were unable to differentiate at a high dosage of GDNF<sup>22</sup>. Despite the deficiency of GDNF in the differentiation of spermatogenic stem cells, we speculate whether, if GDNF could increase stem cell migration and homing of AFSCs in damaged kidneys, the therapeutic potential of AFSCs for renal interstitial fibrosis could be enhanced by cell pretreatment with the *GDNF* gene.

## Materials and Methods

### AFSC Culture

Samples of human amniotic fluid were obtained from women at 15–20 weeks of gestation for prenatal diagnosis after they signed written informed consent. The amniotic fluid was centrifuged at 1200 rpm for 5 min. Sedimentary cells were cultured in Dulbecco's Modified Eagle's Medium/F12 (Gibco/BRL, Grand Island, NY, USA) supplemented with 15% fetal bovine serum (Gibco/BRL), 4 ng/ml basic fibroblast growth factor (bFGF) (R&D Systems, Minneapolis, MN, USA), 100 mg/ml glutamine (Sigma-Aldrich, St. Louis, MO, USA) and 1% penicillin-streptomycin antibiotics (Gibco/BRL), plated in 25 cm<sup>2</sup> T-flasks, and

maintained at 37°C in a 5% CO<sub>2</sub> incubator. The culture medium was changed every 2 or 3 days.

### Immunomagnetic Bead Sorting

According to a previous report<sup>23</sup>, the primary passage of amniotic fluid cells was selected through immunomagnetic bead sorting using a CD117 MicroBead Kit (Miltenyi Biotec, Bergisch Gladbach, North Rhine-Westphalia, Germany). The sorted cells were cultured as before. AFSCs were subcultured at a dilution of 1:3 at 80–90% confluence.

### Lentivirus Vector Transfection

Lentiviral vectors with GDNF-green fluorescent protein (GFP) genes (Lv-GDNF-GFP) or without GDNF genes (Lv-GFP) were constructed by the Ji Kai Gene Company (Shanghai, China). Cultured AFSCs at the third passage were transfected with Lv-GDNF-GFP and Lv-GFP at the most appropriate multiplicity of infection (MOI = 20) following standard procedures. GFP expression was observed at 1, 3, and 5 days of transfection under a fluorescence microscope.

### Animal Model and Treatment

Nu/nu mice (body weight: 18–22 g, age: 6–8 weeks) were purchased from the Laboratory Animal Centre of Xuzhou Medical University (Jiangsu, China). The animals were maintained in a temperature- (22 ± 1°C) and light- (12 h light–dark cycle) controlled room with free access to food and water. After 1 week of acclimation, the mice were divided randomly into sham operated mice (sham group), unilateral ureteral obstruction (UUO) mice treated with intravenous injection of saline solution (UUO group), UUO mice treated with intravenous injection of AFSCs immediately after UUO (AFSC group), and UUO mice treated with intravenous injection of GDNF-modified AFSCs immediately after UUO (GDNF-AFSC group), and sacrificed at days 3 and 7 post-surgery (six in each group). UUO was performed using an established procedure as described<sup>24</sup>. The animals in the AFSC group were injected intravenously through the tail vein with 3.5 × 10<sup>5</sup> GFP labeled AFSCs in 150 µl of PBS, and the GDNF-AFSC group was injected with 3.5 × 10<sup>5</sup> GFP labeled GDNF-AFSCs in 150 µl of PBS via the same route. As a control, the animals in the UUO group were injected with a saline solution. At days 3 and 7 post-surgery, mice were sacrificed. The left kidneys were extracted and washed in saline solution. One part of the kidneys was fixed in 10% formaldehyde for immunohistochemical staining, while the other part was stored at –80°C for later Western blot analysis.

### Transmission Electron Microscopy

The 1-mm<sup>3</sup> renal cortex tissues were fixed in cold 2.5% glutaraldehyde for 4 h. The renal tissue was post-fixed in 1% osmium tetroxide for 2 h, and then immersed in acetone

and ethanol (first: acetone: epoxy resin (2:1), second: acetone: epoxy resin (1:2)), taking 2 h for each step. The embedding mold was filled with epoxy resin, and the renal tissue was immersed at the top of the mold and embedded for 2 h. A knife and microscope were used to expose the tissue to the surface of block. Then, ultrathin sections 60–90 nm thick were placed onto copper nets. The sections were washed with 1% uranyl acetate (1 h) and 0.5% lead citrate (10–15 min). The sections were then examined and photographed with an FEI Tecnai G2 transmission electron microscope.

### Immunofluorescence Labeling

AFSCs, both untreated and modified with GDNF, were labeled with GFP and injected into UUO mice. The tissues were fixed in 4% paraformaldehyde for 48 h and subsequently dehydrated in 30% sucrose for 2 days. Kidney samples were embedded in OCT and sectioned in 10- $\mu$ m-thick slices by Leica CM1950, a frozen section machine, according to the manufacturer's instructions. Selected sections were incubated with 10% donkey serum in PBS containing 0.3% Triton-X-100 for 2 h at room temperature. The sections were then incubated with rabbit anti-OCT-4 polyclonal antibody (1:50, Wuhan, China) at 4°C for 24h. All sections were then observed using a fluorescence microscope. Alexa 594 goat anti-rabbit IgG (1:200, Invitrogen, Carlsbad, CA, USA) was added to the corresponding sections and incubated for 2 h at room temperature. Tissue sections were mounted with 50% glycerol mounting medium. All sections were then visualized with a confocal laser microscope.

### Renal Histology

To evaluate renal morphology, kidney samples were fixed in 10% formaldehyde, embedded in paraffin, sectioned into 4- $\mu$ m-thick sections, deparaffinized and then incubated for 15 min in Histochoice. Subsequently, the sections were sequentially incubated for 5 min in 100% alcohol, 95% alcohol, 85% alcohol, 75% alcohol, and then stained with hematoxylin-eosin and Masson's trichrome. The areas of interstitial fibrosis were detected using Masson's trichrome staining to visualize the collagen fibers, which were stained dark blue. Ten microscopic visual fields of kidney tissues were selected randomly in the sections under high-power magnification ( $\times 40$ ).

### Immunohistochemical Staining

Mouse kidneys were fixed in 4% paraformaldehyde and embedded in paraffin. The paraffin-embedded kidney tissues were sectioned at a thickness of 5  $\mu$ m. Two-step IHC detection was used for the immunohistochemical procedures. The sections were incubated with the following antibodies overnight at 4°C in PBS: goat anti-UCP2 polyclonal antibody (1:100, Abcam, Cambridge, MA, USA), rabbit anti-monocyte chemoattractant protein 1 (MCP1) antibody (1:100, Abcam), mouse anti-NT monoclonal antibody (1:100,

SANTA CRUZ, Dallas, TX, USA), rabbit anti-tumor necrosis factor  $\alpha$  (TNF $\alpha$ ) polyclonal antibodies (1:150, Abcam), rabbit anti-NOX2/gp91phox polyclonal antibodies (1:50, Abcam), rabbit anti-TGF- $\beta$ 1 polyclonal antibodies (1:200, Abcam), rabbit anti-collagen-I (1:200, Abcam), mouse anti-VEGF monoclonal antibodies (1:150, Abcam), and rabbit anti-hypoxia inducible factor-1 $\alpha$  (HIF1- $\alpha$ ) polyclonal antibodies (1:200, Proteintech). After washing, the slides were incubated at 37°C in PV6001 (Zhongshan, Beijing, China), and the sections were then visualized with diaminobenzidine tetrahydrochloride (DAB, Zhongshan) substrate and counterstained with hematoxylin. Ten discontinuous visual fields of the outer cortex of the kidney were also randomly selected under the microscope for each section. The integrated optical density (IOD) total of each visual field was determined using the Image 6 Pro Plus System.

CD34-stained kidney tissue samples were examined under a light microscope at 40 $\times$  magnification to estimate peritubular capillary density as previously described. PTCs that stained positive for CD34 (an endothelial cell-specific marker) were counted in five randomly chosen microscopic fields on each slide, and capillary density was presented as the average number of capillaries/0.065 mm<sup>2</sup>.

### Western Blotting

Kidney tissue samples were lysed and then centrifuged. Approximately 150  $\mu$ g of total protein was loaded on 10% or 12% sodium dodecyl sulfate-polyacrylamide (SDS) gels and transferred to a polyvinylidene difluoride (PVDF) membrane by electroblotting. Non-specific binding was blocked by incubating the membrane in 3% bovine serum albumin (BSA) for 2 h at room temperature. The membrane was then incubated overnight at 4°C with primary antibodies against collagen I, TGF- $\beta$ 1, UCP2, MCP-1, NT, TNF $\alpha$ , gp91phox, HIF1- $\alpha$ , VEGF, optic atrophy protein-1 (OPA-1), and dynamin-related protein-1 (DRP-1), followed by an incubation with alkaline phosphatase-conjugated secondary antibodies. The protein expression levels were detected by a BCIP/NBT Alkaline Phosphatase Color Development Kit. Positive immunoreactive bands were quantified densitometrically and normalized by beta actin.

### Statistical Analyses

Data are presented as the mean  $\pm$  SD, and statistical analysis was performed with SPSS 16.0. Comparisons between groups were analyzed by one-way analysis of variance (ANOVA) followed by Dunnett's post hoc test. A P-value less than 0.05 was considered statistically significant.

## Results

### Culture of AFSCs and Lentivirus Vector Transfection

The selected CD117-positive AFSCs exhibited fibroblastic or needle shapes with larger nuclei (Fig 1a). To determine

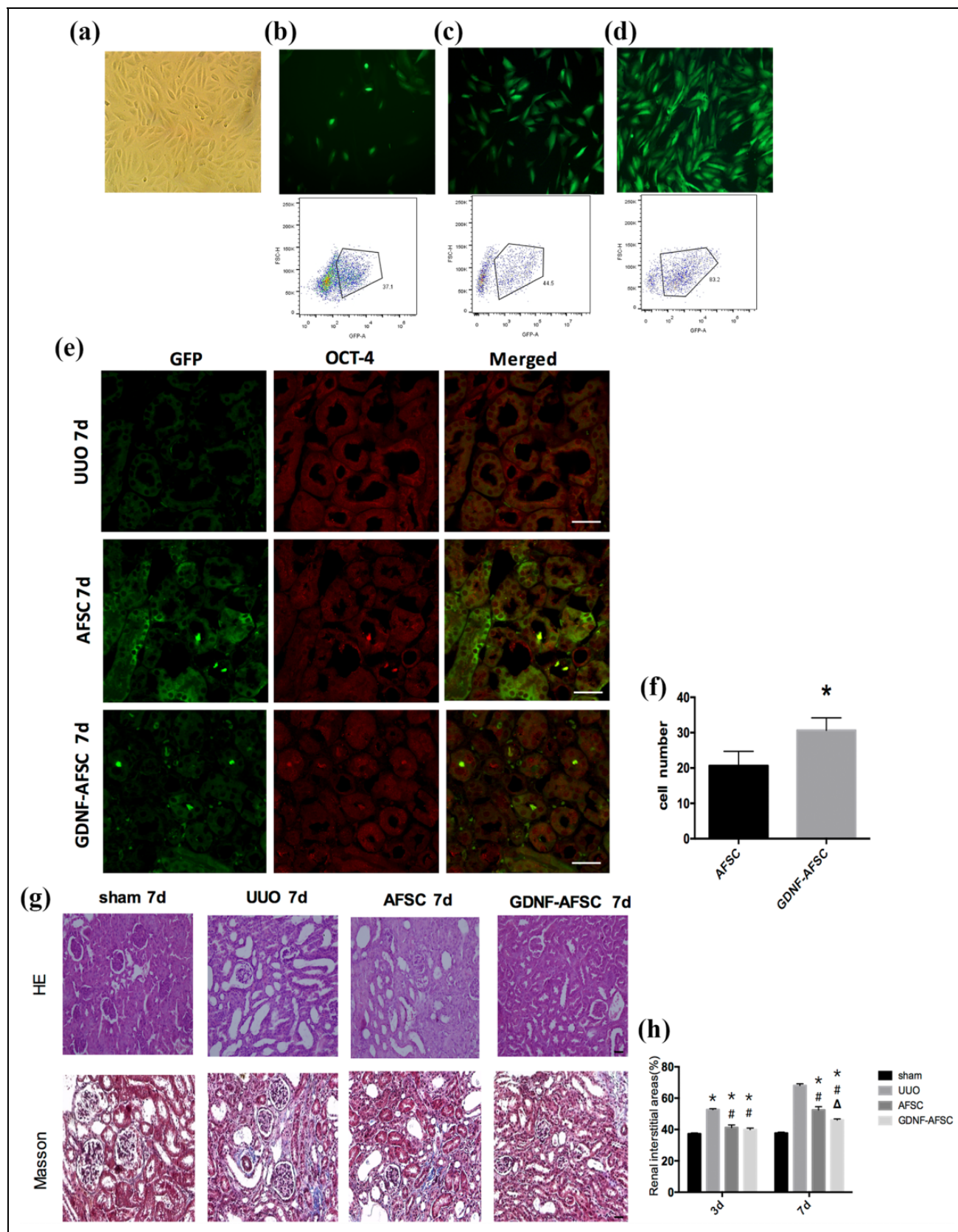


**Fig 1.** Culture of AFSCs, lentivirus vector transfection, and immunofluorescent localization of frozen section in AFSC transplanted kidney. (a) AFSCs exhibited fibroblastic or needle shapes with larger nuclei. Bar = 50  $\mu$ m. (b-d) Fluorescence expression of lentiviral vectors with GDNF-transfected AFSCs at 1 day, 3 days, and 5 days. Low GFP expression was detected at 1 day and gradually increased. For 5 days after

the transfection efficiency, we used fluorescence microscopy to observe the GFP signal. A faint GFP signal was detected at 24 h, and it gradually increased over the course of the transfection. By 5 days after transfection, approximately 83.2% of AFSCs expressed GFP, as indicated by green fluorescence (Fig 1).

### Immunofluorescent Staining of Frozen Sections from AFSC Transplanted Kidney

As shown in Fig 1e and f, the tissue showed no GFP and OCT-4 staining in the UUO group, which is an AFSC marker. AFSCs, indicated by OCT-4 staining and GFP were shown in renal tissues in the AFSC group. Compared with the AFSC group, the tissue treated with AFSCs modified with GDNF exhibited increased OCT-4 staining and GFP, which indicated successful localization of AFSCs and GDNF - AFSCs in the renal interstitium and GDNF could help homing of stem cells to the obstructed kidney.

### Renal Morphology

Renal histology was investigated using hematoxylin-eosin and Masson's trichrome staining. As shown in Fig 1g and h, there was no significant histological abnormality in the sham group. After unilateral ureteral occlusion, severe morphological lesions and ECM production were detected. Compared with UUO, the AFSC and GDNF-AFSC groups, especially the latter, showed less renal fibrosis.

### Immunohistochemical Staining and Western Blot Analysis of Nitrotyrosine (NT), Anti-uncoupling Protein 2, and Gp91phox Expression Levels

As shown in Fig 2, low NT, UCP2, and gp91phox expression levels were detected in the sham group. Immunohistochemistry revealed that NT, UCP2 and gp91phox were increased in the UUO group compared with those in the sham-operated group, decreased in the AFSC group compared with those in the UUO group, and further decreased in the GDNF-AFSC group (Fig. 3a–c). Western blot analysis results showed that gp91phox and NT protein levels were higher in the UUO group than in the sham group ( $P < 0.001$  vs. sham), decreased in the AFSC group, and further decreased in the GDNF-AFSC group ( $P < 0.001$  vs. UUO). Meanwhile, there were no significant differences in UCP2 expression at day 3

post-surgery within the UUO, AFSC, and GDNF-AFSC groups ( $P > 0.05$ ). However, UCP2 protein expression was increased in fibrotic kidneys at day 7 in the UUO group compared with that in the sham-operated kidneys ( $P < 0.001$  vs. sham). After the AFSCs and GDNF-AFSCs treatments, the expression of UCP2 was significantly decreased ( $P = 0.001$  and  $P < 0.001$  vs. UUO, respectively), particularly in the GDNF-AFSC group ( $P < 0.001$  vs. AFSC). These data demonstrate the superior anti-oxidative effect of GDNF-modified AFSCs.

### Immunohistochemical Staining and Western Blot Analysis of MCP1 and TNF $\alpha$ Expression Levels

We found light MCP1 and TNF $\alpha$  staining in the sham group. The expression levels of these pro-inflammatory cytokines were upregulated at days 3 and 7 post-surgery in the UUO group compared with the sham group, decreased in the AFSC group and further decreased in the GDNF-AFSC group (Fig 3a and b). Western blotting revealed similar trends in the protein expression levels of MCP1 and TNF $\alpha$  to those observed by immunohistochemistry (Fig 3c and d). However, there were no significant differences in MCP1 and TNF $\alpha$  expression levels at day 3 post-surgery between the AFSC and GDNF-AFSC groups ( $P = 0.086$ ,  $P = 0.168$ ). The expression levels of MCP1 and TNF $\alpha$  were increased at day 7 in the UUO group compared with the sham group ( $P < 0.001$  vs. sham), while the levels were significantly decreased in the AFSC group and GDNF-AFSC group compared with the UUO group ( $P < 0.001$  vs. UUO), especially in the GDNF-AFSC group ( $P < 0.001$  vs. AFSC). These data demonstrate the greater anti-inflammatory effect of GDNF-AFSCs treatment compared with AFSCs.

### Immunohistochemical Staining of CD34, VEGF, and HIF-1 $\alpha$ , and Western Blot Analysis of VEGF and HIF-1 $\alpha$ Expression Levels

CD34 is a marker of endothelial cells. In the sham group, PTCs were uniform in size and shape, and the expression of VEGF was distributed normally throughout the tubular epithelial cells. At days 3 and 7 after surgery, there was a significant decrease in PTC density and VEGF staining in the UUO group. However, PTC density and VEGF staining were stronger in the AFSC group than in the UUO group, and these increases were further augmented in the GDNF-AFSC

**Fig 1.** (Continued). transfection, approximately 83.2% of AFSCs expressed the GFP gene, which is indicated by green fluorescence. Bar = 50  $\mu$ m. (e,f) AFSCs were visualized in the AFSC and GDNF-AFSC groups by GFP and OCT-4 staining (appear green and red, respectively). AFSCs are GFP + and OCT-4+ (colocalization appears as yellow-green; arrows). Compared with the AFSC group, the tissue treated with AFSCs modified with GDNF exhibited increased GFP and OCT-4 staining. Bar = 20  $\mu$ m. (g) Representative micrographs of hematoxylin-eosin and Masson's trichrome staining demonstrate histological changes in the indicated groups. (h) Renal interstitium areas in each group. Fibrosis increased in UUO compared with sham, decreased in the AFSC group compared with the UUO group, and further decreased in the GDNF-AFSC group compared with the AFSC group. Bar = 20  $\mu$ m. (\* $P < 0.05$  vs. sham group; # $P < 0.05$  vs. UUO group;  $\Delta P < 0.05$  vs. AFSC group).



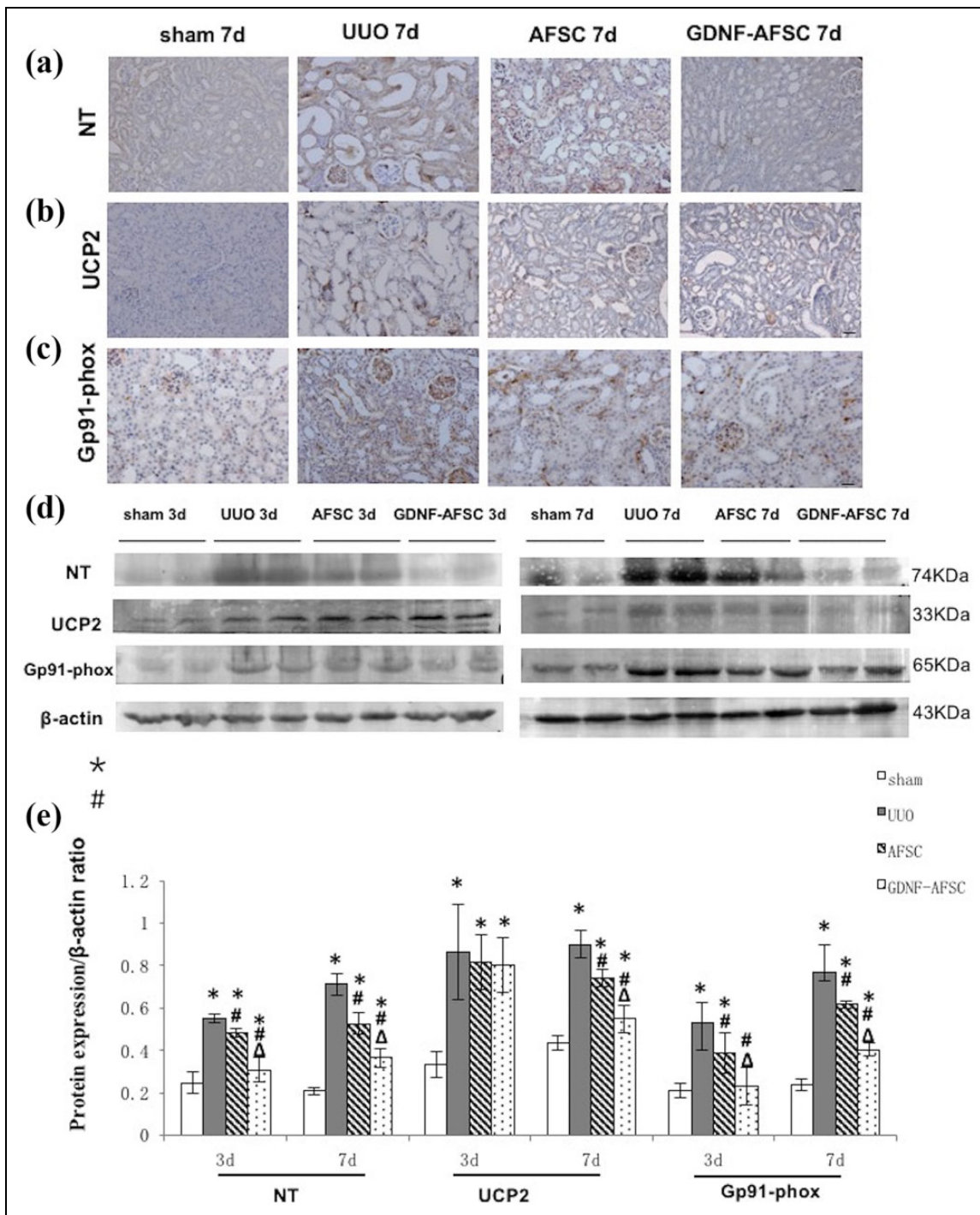


**Fig 2.** Immunohistochemical staining and Western blot analysis of nitrotyrosine (NT), UCP2, and gp91 phox. (a–c) NT, UCP2, and gp91 phox staining was increased in the UUO group at day 7 post-surgery compared with that in the sham group and decreased in the AFSC and GDNF-AFSC groups compared with that in the UUO group, especially in the GDNF-AFSC group. Bar = 20  $\mu$ m. (d) Representative (2 bands shown per group) immunoblotting of NT, gp91 phox, and UCP2. (e) The expression levels of NT, gp91 phox, and UCP2 were elevated in the UUO group at day 7, whereas the levels were decreased in the AFSC group and further decreased in the GDNF-AFSC group. There were no significant differences in UCP2 expression at day 3 post-surgery within the UUO, AFSC, and GDNF-AFSC groups (\* $P$  < 0.05 vs. sham group; # $P$  < 0.05 vs. UUO group;  $\Delta P$  < 0.05 vs. AFSC group).

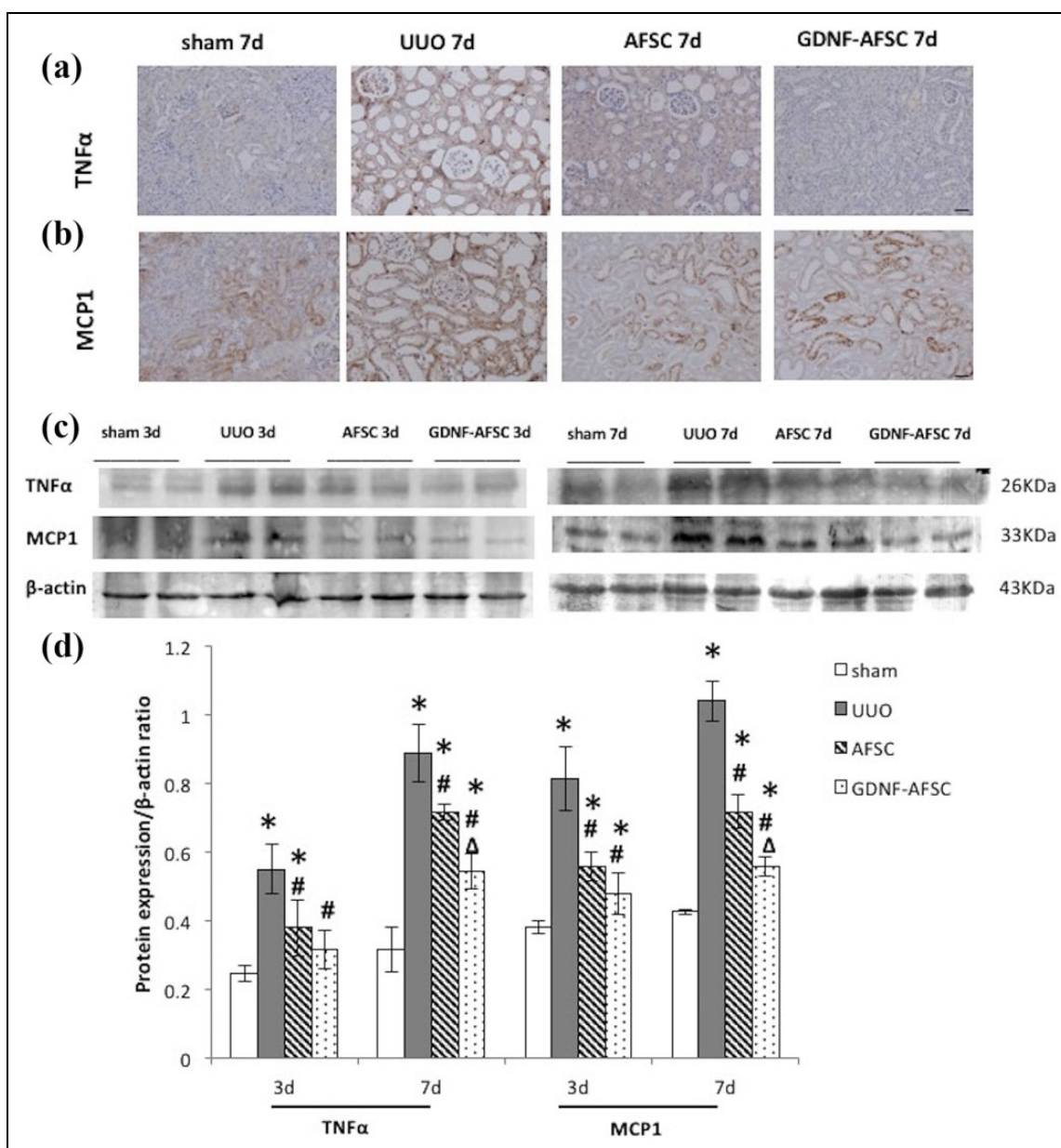


**Fig 3.** Immunohistochemical staining and Western blot analysis of TNF $\alpha$  and MCP1. (a, b) TNF $\alpha$  and MCP1 staining was increased in the UUO group compared with that in the sham group at day 7 post-surgery, whereas the staining was decreased in the AFSC group compared with that in the UUO group and further decreased in the GDNF-AFSC group. Bar = 20  $\mu$ m. (c) Representative (2 bands shown per group) immunoblotting of TNF $\alpha$  and MCP1. (d) The expression levels of TNF $\alpha$  and MCP1 were elevated in the UUO group and decreased in the AFSC and GDNF-AFSC groups, especially in the GDNF-AFSC group. (\* $P < 0.05$  vs. sham group; # $P < 0.05$  vs. UUO group;  $\Delta P < 0.05$  vs. AFSC group).

group at each time point. Western blot analysis revealed similar trends in VEGF protein levels to those observed in the immunohistochemistry results (Fig 4d). These results suggest that GDNF-AFSC transplantation may further promote angiogenesis in obstructed kidneys.

In the sham group, there was faint HIF-1 $\alpha$  staining in cortical nuclei and stronger staining in distal tubules (Fig 4c). HIF-1 $\alpha$  expression increased owing to the rarefaction of the PTC in the UUO group compared with that in the

sham group. However, compared with the UUO group, the AFSC group exhibited dramatically decreased HIF-1 $\alpha$  expression, which was further decreased after GDNF-AFSCs injection. Western blot analysis (Fig 4d) showed that the levels of HIF-1 $\alpha$  decreased in the AFSC group at days 3 and 7 post-surgery compared with the UUO group at each time point ( $P < 0.001$  vs. UUO) and remained even lower in the GDNF-AFSC group than in the AFSC group ( $P < 0.001$  vs. AFSC). These results demonstrate that GDNF-

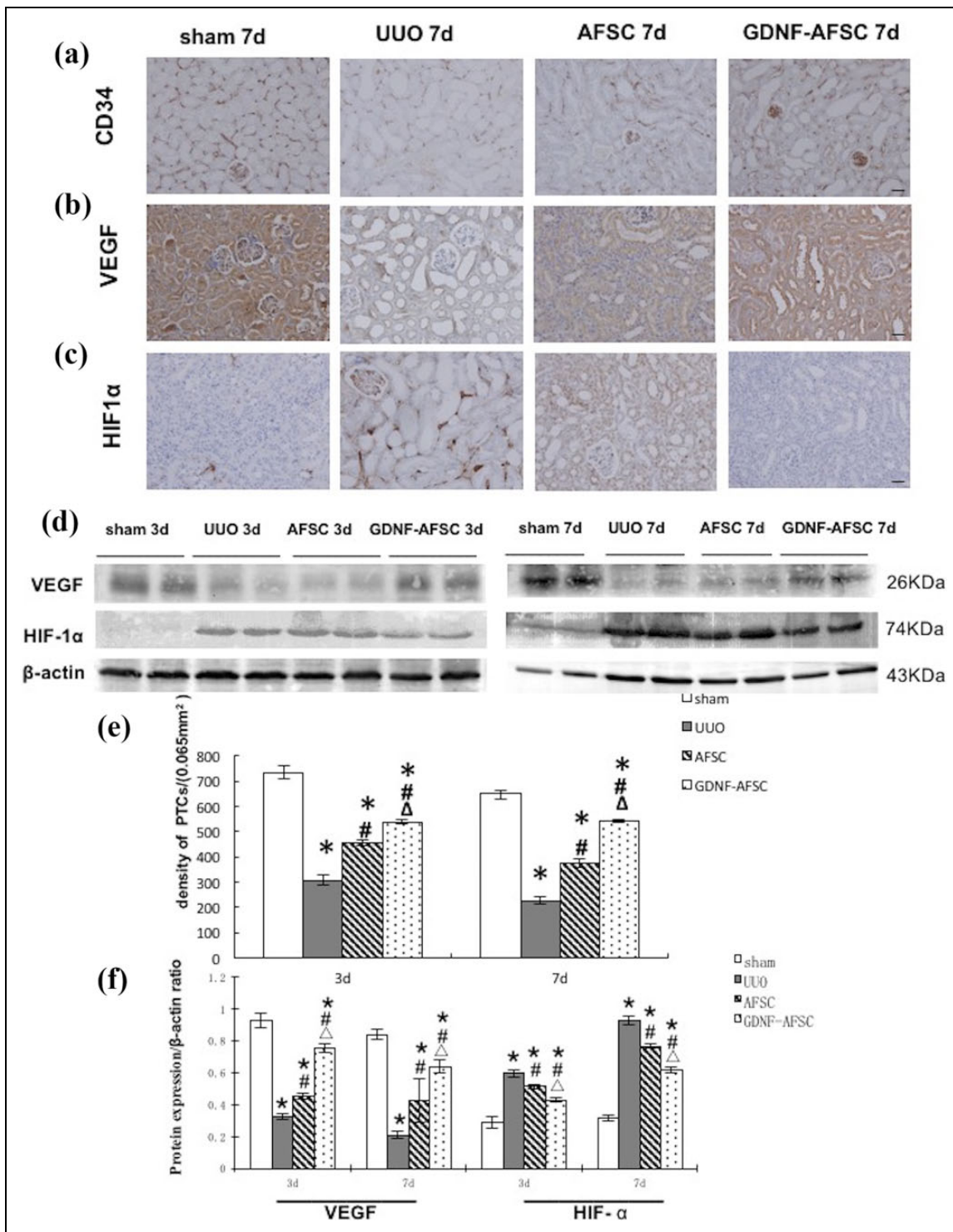


**Fig 4.** Immunohistochemical staining of CD34, VEGF, and HIF-1 $\alpha$  and Western blot analysis of VEGF and HIF-1 $\alpha$  expression. (a, b) CD34 and VEGF staining was decreased in the UUO group compared with that in the sham group at day 7 post-surgery, whereas the staining was increased in the AFSC group compared with that in the UUO group and further increased in the GDNF-AFSC group. Bar = 20  $\mu$ m. (c) HIF-1 $\alpha$  expression was increased in the UUO group compared with that in the sham group, while the expression was decreased in the AFSC group compared with the UUO group and further decreased in the GDNF-AFSC group. (d) Representative (2 bands shown per group) immunoblotting of VEGF and HIF-1 $\alpha$ . (e, f) CD34 and VEGF expression levels were decreased in the UUO group, increased in the AFSC group and further increased in the GDNF-AFSC group. The hypoxia marker was elevated in the UUO group and decreased in the AFSC and GDNF-AFSC groups, especially in the GDNF-AFSC group. (\*P < 0.05 vs. sham group; #P < 0.05 vs. UUO group;  $\Delta$ P < 0.05 vs. AFSC group).



AFSC transplantation alleviates the hypoxic conditions associated with obstructed kidney.

### TEM of Mitochondria

To further evaluate the effect of GDNF-AFSCs on UUO-induced renal interstitial fibrosis *in vivo*, the morphology of renal mitochondria was observed by TEM. As shown in Fig 5a, the mitochondrial configuration was normal, and the mitochondrial cristae, which result from folds in the inner mitochondrial membrane into the matrix, were arranged closely in the sham group. However, mitochondrial swelling and mitochondrial cristae fragmentation or disappearance were commonly seen in the UUO model. Meanwhile, all pathological characteristics were alleviated in the AFSC group, especially in the GDNF-AFSC group.

### Western Blot Analysis of OPA-1 and DRP-1 Expression Levels

As shown in Fig 5b and c, OPA-1 protein expression was highest in the sham group. However, OPA-1 expression was decreased at days 3 and 7 in the UUO group ( $P < 0.001$  vs. sham). Compared with the UUO group, the AFSC group exhibited increased OPA-1 expression ( $P < 0.001$  vs. UUO), which was further increased in the GDNF-AFSC group at each time point ( $P < 0.001$  vs. AFSC). The expression of DRP-1 was increased at days 3 and 7 in the UUO group compared with that in the sham group ( $P < 0.001$  vs. sham), significantly decreased in the AFSC group ( $P < 0.001$  vs. UUO), and further decreased in the GDNF-AFSC group at each time point ( $P < 0.001$  vs. AFSC).

### Immunohistochemical Staining of TGF- $\beta$ 1 and Collagen-I and Western Blot Analysis of TGF- $\beta$ 1 Expression

Immunohistochemical staining showed that the expression levels of TGF- $\beta$ 1 and collagen-I were significantly increased in the UUO group compared with those in the sham-operated kidney at both days 3 and 7 post-surgery. Both AFSCs and GDNF-AFSCs treatments decreased UUO-induced TGF- $\beta$ 1 expression and collagen fibril deposition, and the effect of GDNF-AFSCs was even greater than that of AFSCs (Fig. 6a). Western blot analysis showed that the expression of TGF- $\beta$ 1 was upregulated in the UUO group compared with that in the sham group ( $P < 0.001$  vs. sham), decreased in the AFSC group ( $P < 0.001$  vs. UUO) and even lower in the GDNF-AFSC group ( $P < 0.001$  vs. AFSC). These data suggest that GDNF-modified AFSCs can alleviate renal fibrosis.

### Discussion

Here, we found that oxidative stress and inflammation were induced by obstructive nephropathy. These changes were

accompanied by PTC injury and severe hypoxia, which might contribute to mitochondrial damage and renal injury progression. However, the GDNF gene can promote the ability of AFSCs to inhibit inflammation and oxidative stress, which ultimately ameliorate renal fibrosis.

The prevalence of CKD worldwide is rising, with many factors contributing to kidney injury<sup>25</sup>, and interstitial fibrosis is regarded as the main pathway of CKD. Although numerous researchers have made great efforts to explore the mechanisms of CKD over the last several decades, current methods for CKD treatment are still ineffective. Therefore, a better understanding of the pathogenesis of CKD and methods to arrest the progression of renal fibrosis are urgently needed. In this study, we demonstrated that, compared with AFSCs, GDNF-modified AFSCs were more effective at ameliorating renal fibrosis by inhibiting oxidative stress and inflammation.

AFSCs, a novel population of broadly multipotent stem cells that exhibit both embryonic and adult stem cell characteristics, have been regarded as a promising approach for cell therapy<sup>16</sup>. Our group has demonstrated that transplanting AFSCs into mice with ureteral ligation accelerated the proliferation of tubular epithelial cells and ameliorated renal interstitial fibrosis<sup>15</sup>. Our current study also showed that AFSCs can accelerate renal recovery in mice after UUO through anti-inflammatory and anti-oxidative mechanisms. The renal differentiation capacity of AFSCs is not very powerful, so we explored a potential method to strengthen the ability of AFSCs to alleviate renal interstitial fibrosis.

GDNF, a neurotrophic factor that has the ability to participate in early nephrogenesis<sup>26,27</sup>, can induce AFSCs to move toward the peritubular compartment and can promote the survival of stem cells in response to hypoxic, inflammatory, and oxidative conditions. Our experiments<sup>28</sup> validated the above-mentioned findings and revealed that preconditioning AFSCs with GDNF gene can enhance their migration, engraftment, survival, and, consequently, maximize the effect of common AFSC transplantation.

Oxidative stress has also been implicated in the pathogenesis of renal fibrosis<sup>29-31</sup>. Several studies<sup>32</sup> have demonstrated that many factors that induce renal fibrosis are associated with an increase in oxidative stress, resulting in increased ROS, which contribute to lipid peroxidation, increased hydrogen peroxide, and DNA and protein damage. The expression levels of oxidative stress markers, including gp91-phox, NT, and UCP2, which are increased in UUO models, were observed in the present study. Gp91-phox, also known as NOX2, is the predominant NOX family subunit in the kidney. Gp91-phox is a major source of ROS and plays a critical role in transferring electrons through the enzyme from NADPH to molecular oxygen to produce superoxide, subsequently leading to tissue damage<sup>33</sup>. Compared with AFSCs, GDNF-modified AFSCs had a stronger inhibitory effect on the levels of gp91-phox, suggesting that GDNF-AFSCs may represent a renoprotective capacity for obstructed kidneys. These effects are possibly associated

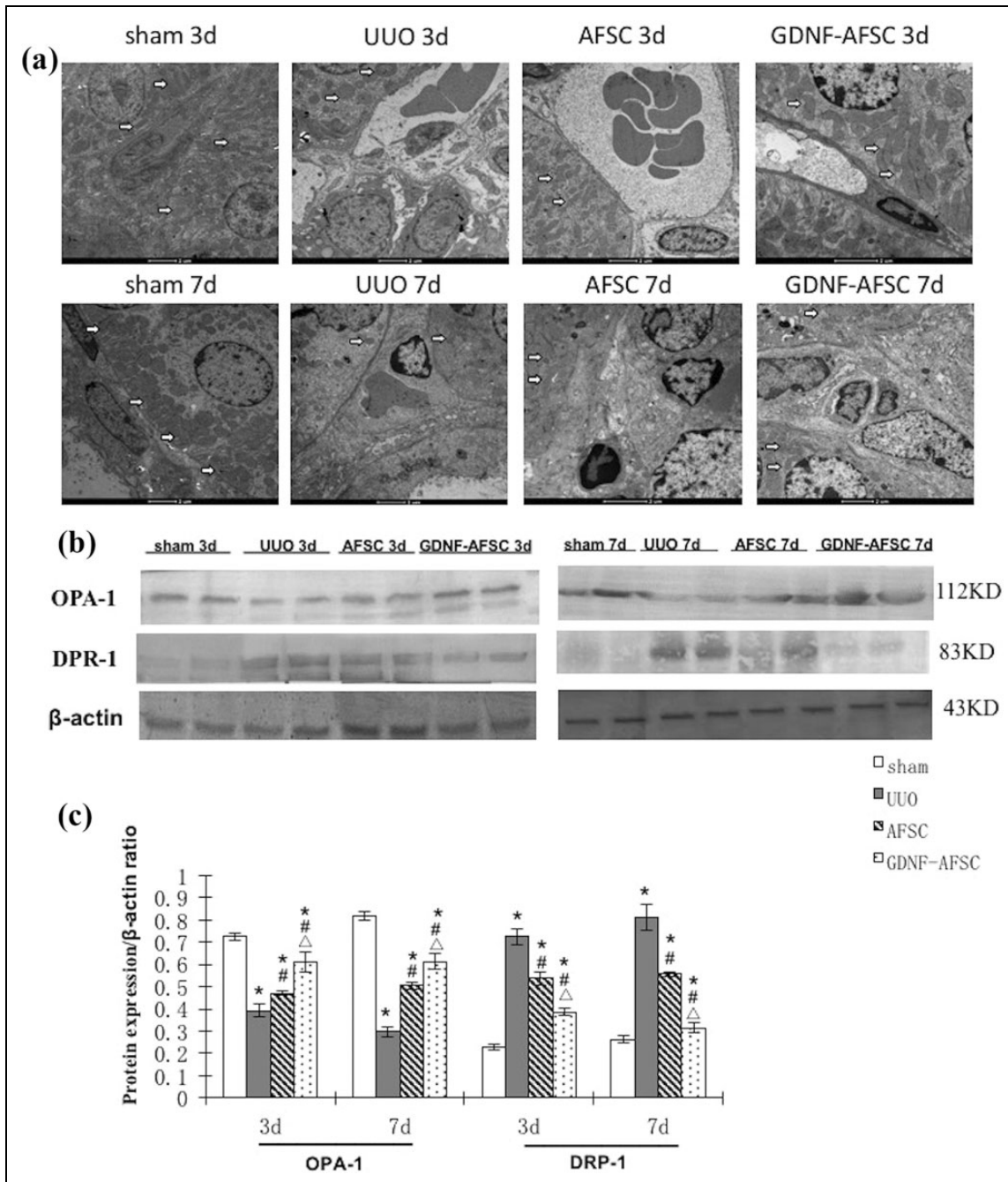


**Fig 5.** TEM images of mitochondria and Western blot analysis of OPA-1 and DRP-1. (a) There was no mitochondrial injury in the sham group at days 3 and 7 post-surgery. However, mitochondrial swelling and mitochondrial cristae fragmentation or disappearance were commonly seen in the UUO model. Meanwhile, all those pathological changes were ameliorated in the AFSC group, especially in the GDNF-AFSC group. Bar = 2 μm (b) Representative (2 bands shown per group) immunoblotting of OPA-1 and DRP-1. (c) OPA-1 expression levels were decreased in the UUO group compared with those in the sham group at days 3 and 7 post-surgery, while the levels were increased in the AFSC group and further increased in the GDNF-AFSC group. DRP-1 was elevated in the UUO group compared with that in the sham group, while decreased in the AFSC group and further decreased in the GDNF-AFSC group. (\* $P < 0.05$  vs. sham group; # $P < 0.05$  vs. UUO group; Δ $P < 0.05$  vs. AFSC group).

with the attenuation of NOX2-dependent oxidative stress. Another oxidative stress marker, NT, is used as an indirect indicator of peroxynitrite, which possesses a short biological half-life and specifically nitrates tyrosine residues on

proteins<sup>34</sup>. Nitric oxide (NO) reacts with superoxide anion to generate peroxynitrite. In addition, NO has been identified as a significant mediator involved in the physiopathology of renal fibrosis<sup>35</sup>. Our study showed that GDNF-AFSCs

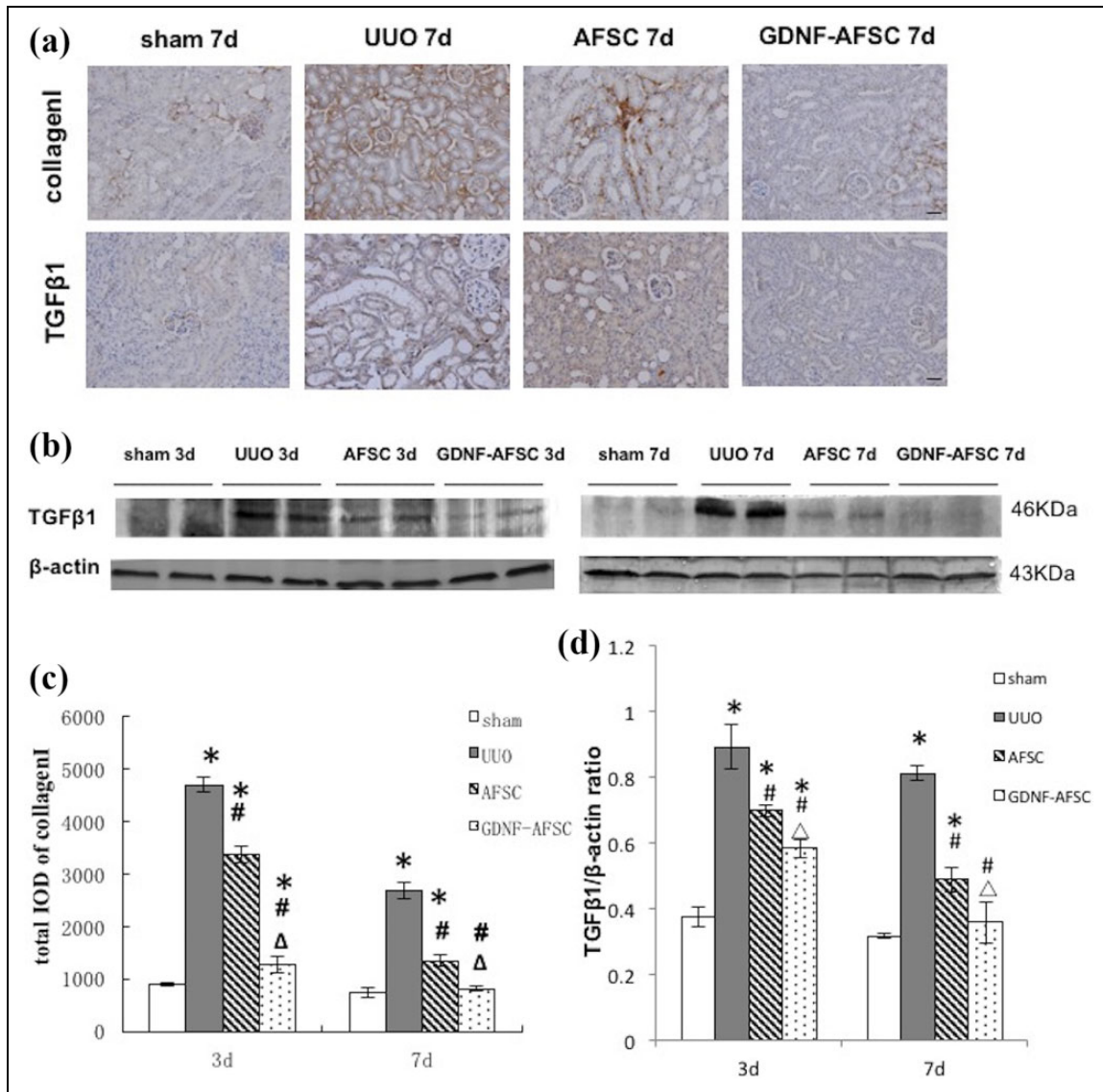


**Fig 6.** Immunohistochemical staining of TGF-β1 and collagen-I and Western blot analysis of TGF-β1. (a, c) TGF-β1 and Collagen-I were increased in the UUO group compared with those in the sham group at day 7 post-surgery, whereas these markers were decreased in the AFSC group compared with those in the UUO group and further decreased in the GDNF-AFSC group compared with those in the AFSC group. Bar = 20 μm. (b, d) Representative (2 bands shown per group) immunoblotting of TGF-β1. The fibrotic marker was elevated in the UUO group and decreased in the AFSC and GDNF-AFSC groups at each time point, especially in the GDNF-AFSC group. (\*P < 0.05 vs. sham group; #P < 0.05 vs. UUO group; ΔP < 0.05 vs. AFSC group).

decreased the expression of NT in obstructed kidneys and exhibited more effective anti-oxidative stress abilities than AFSCs. UCP2 is a mitochondrial inner membrane protein that regulates proton conductance. Mitochondrial dysfunction induced by stimulation such as hypoxia and oxidative stress, will lead to the upregulation of UCP2 levels. According to previous studies<sup>36</sup>, the expression of UCP2 is increased in many diseased conditions, such as diabetes, hypertension, atherosclerosis, and, in our experimental model, renal interstitial fibrosis. However, compared with untreated fibrotic kidneys, kidneys treated with AFSCs and GDNF-AFSCs exhibited markedly reduced pathological

effects at day 7, particularly kidneys in the GDNF-AFSC group. Meanwhile, the antioxidative effect of AFSCs and GDNF-AFSCs was not obvious in the UUO group at day 3 post-surgery, but the reason is unclear. These results indicate that GDNF-AFSCs played a larger role in the amelioration of renal fibrosis through anti-oxidative effects.

In recent years, renal inflammation has been increasingly recognized in the progression of renal fibrogenesis<sup>5,37</sup>, particularly in association with cytokine release and chemokine expression<sup>1</sup>. Previous studies<sup>38,39</sup> have indicated that the renal fibrosis induced by UUO models is characterized by inflammatory cell recruitment,

macrophage infiltration, and increased pro-inflammatory cytokines. In addition, infiltration of inflammatory cells is also consistent with the degree of renal fibrosis<sup>6,40</sup>. Therefore, pro-inflammatory cytokines have been considered contributors to the progression of renal interstitial fibrosis. Our present study showed that TNF $\alpha$  and MCP1, the major pro-inflammatory cytokines, were increased in UUO kidneys. However, the injection of AFSCs noticeably downregulated the increase in chemokines and inflammatory cytokines, and GDNF-AFSCs can further reduce the expression levels of TNF $\alpha$  and MCP1, which suggests that the decrease in pro-inflammatory cytokines seen in renal fibrosis may due to its anti-inflammatory effects.

VEGF is a specific endothelial growth factor that can promote peritubular capillary repair and angiogenesis<sup>15</sup>. Several studies have confirmed that VEGF can maintain the integrity of the kidney vascular endothelial cells by regulating renal microvessels<sup>41</sup>. The detection of decreased VEGF levels in UUO could be the result of multiple factors, including inflammation and oxidative stress. However, the levels of VEGF in the AFSC and GDNF-AFSC group were higher than those in the UUO group, while VEGF levels were more significantly upregulated in the GDNF-AFSC group. PTC injury is known to be associated with reduced blood supply, leading to chronic ischemia and hypoxia<sup>42,43</sup>. PTC-positive areas, which were determined based on CD34 immunostaining in the present study, showed that the PTCs were damaged in the UUO group. The rarefaction of the PTCs in turn results in tissue hypoxia, which was suggested by the upregulation of HIF-1 $\alpha$ <sup>44</sup>. Our study showed that both AFSC and GDNF-AFSC transplantation had the ability to repair renal blood vessels, stimulate an increase in PTC density, and alleviate tissue hypoxia, while GDNF-AFSC transplantation had a stronger effect. The oxygen insufficiency in the interstitium results from serious damage to renal tubular epithelial cells and a subsequent decrease in PTC density. Under hypoxia, renal tubular epithelium cells undergo epithelial-mesenchymal transitions. These cells can migrate to the interstitium and differentiate into myofibroblasts and promote ECM production, such as collagen<sup>45</sup>. The final effect of this process is renal interstitial fibrosis. Our findings indicate that the transplantation of GDNF-AFSCs into UUO mice was more effective at ameliorating hypoxia and subsequently alleviating the degree of renal fibrosis. The mechanisms involved in this process appear to be directly related to the anti-inflammatory and anti-oxidative effects of GDNF-AFSCs.

A growing number of studies have suggested that chronic ischemia and hypoxia due to oxidative stress and inflammation are associated with mitochondrial injury<sup>46</sup>. Mitochondria are the main organelles in eukaryotic cells, playing an important role in cellular energy production and providing most of the energy for cellular physiological needs. Mitochondrial morphological dynamics are controlled by a balance between two opposing processes: fission and fusion<sup>47</sup>. OPA-1, a major mitochondrial fusion protein, helps

determine the shape and structure of mitochondria. Our results showed that decreased OPA-1 expression induced by obstructed kidneys was upregulated in the AFSC and GDNF-AFSC groups, especially in the GDNF-AFSC group, indicating that GDNF-AFSCs may promote mitochondrial fusion activity. DRP-1, a major mitochondrial fission protein, is required to induce mitochondrial fragmentation and programmed cell death. Our study showed that, compared with AFSCs, GDNF-AFSCs achieved a greater reduction in DRP-1 expression. Meanwhile, as TEM showed, mitochondrial swelling and mitochondrial cristae fragmentation or disappearance induced by UUO were ameliorated after the mice were administered GDNF-AFSCs. These results suggest that GDNF-modified AFSCs can alleviate mitochondrial injury and ultimately ameliorate renal interstitial fibrosis.

We chose the UUO mouse as the experimental model in this study. We found typical features of obstructed nephropathy, such as tubular dilation and atrophy, interstitial fibrosis and upregulation of collagen-I deposition and TGF $\beta$ 1 levels<sup>48</sup>. TGF- $\beta$ 1 is a profibrotic mediator that plays a major role in fibrosis, activation of myofibroblasts, and accumulation of ECM<sup>43,49,50</sup>. In the obstructed kidneys, the morphological changes were accompanied by increased expression of collagen-I, a structural component of the ECM, which indicates the progression of renal fibrosis. AFSCs treatment significantly alleviated UUO-induced TGF- $\beta$ 1 and collagen-I expression levels, while the expression levels in the GDNF-AFSC group were lower than those in the AFSC group.

From the above discussion, we can conclude that the *GDNF* gene has the ability to promote the anti-inflammatory and anti-oxidative effects of AFSCs, and GDNF-AFSCs are more effective than AFSCs at ameliorating renal interstitial fibrosis.

### Author Contributions

Conceptualization, S.D.; investigation, S.D.; methodology, L.S.L., Z.Y., W.Z.J., and W.J.; resources, L.C.X.; writing – original draft, L.S.L.; writing – review and editing, S.D. and L.S.L.; funding acquisition, S.D.; supervision, S.D. and L.C.X.; project administration, S.D. Shulin Li and Yuan Zhao contributed equally to this work.

### Ethical Approval

This study was approved by the Institutional Review Board of the Affiliated Hospital of Xuzhou Medical University.

### Statement of Human and Animal Rights

All animal experiments were performed by procedures approved by the Ethics Committee for Animal Research at the Xuzhou Medical University.

### Statement of Informed Consent

There are no human subjects in this article and informed consent is not applicable.



## Declaration of Conflicting Interests

The author(s) declared no potential conflicts of interest with respect to the research, authorship, and/or publication of this article.

## Funding

The author(s) disclosed receipt of the following financial support for the research, authorship, and/or publication of this article: This study was partially supported by a project of the National Natural Science Foundation of China (81270769); a project of the Jiangsu Provincial Natural Science Foundation (BK20161172); a project of “Qing Lan” of Jiangsu Province; a project of the Jiangsu Provincial Commission of Health and Family Planning (H201628); a project of “Liu Ge Yi” of Jiangsu Province; the project of “Liu Da Ren Cai Gao Feng” of Jiangsu Province, China (WSN-113, 2010-WS043); a project of the Technology Development Foundation of Kuitun City (201134); the Jiangsu Overseas & Training Program for University Prominent Young & Middle-aged Teachers and Presidents; and a project of “shi er wu ke jiao xing wei” Key Medical Personnel of Jiangsu Province (RC2011116), a school class project of Xuzhou Medical University (2017KJ13); a project of Jiangsu Provincial Post Graduate Innovation Plan (KYCX17\_1708).

## References

- Wang Y, Wang B, Du F, Su X, Sun G, Zhou G, Bian X, Liu N. Epigallocatechin-3-gallate attenuates oxidative stress and inflammation in obstructive nephropathy via NF-kappaB and Nrf2/HO-1 signalling pathway regulation. *Basic Clin Pharmacol Toxicol*. 2015;117(3):164–172.
- Ai J, Nie J, He J, Guo Q, Li M, Lei Y, Liu Y, Zhou Z, Zhu F, Liang M, et al. GQ5 Hinders renal fibrosis in obstructive nephropathy by selectively inhibiting TGF-beta-induced Smad3 phosphorylation. *J Am Soc Nephrol*. 2015;26(8):1827–1838.
- Zeisberg M, Neilson EG. Mechanisms of tubulointerstitial fibrosis. *J Am Soc Nephrol*. 2010;21(11):1819–1834.
- Rojas-Rivera J, Ortiz A, Egido J. Antioxidants in kidney diseases: The impact of bardoxolone methyl. *Int J Nephrol*. 2012;2012:321714.
- Impellizzeri D, Esposito E, Attley J, Cuzzocrea S. Targeting inflammation: New therapeutic approaches in chronic kidney disease (CKD). *Pharmacol Res*. 2014;81:91–102.
- Chuang ST, Kuo YH, Su MJ. KS370G, a caffeamide derivative, attenuates unilateral ureteral obstruction-induced renal fibrosis by the reduction of inflammation and oxidative stress in mice. *Eur J Pharmacol*. 2015;750:1–7.
- Cheng X, Zheng X, Song Y, Qu L, Tang J, Meng L, Wang Y. Apocynin attenuates renal fibrosis via inhibition of NOXs-ROS-ERK-myofibroblast accumulation in UUO rats. *Free Radic Res*. 2016;50(8):840–852.
- Zheng G, Lyons JG, Tan TK, Wang Y, Hsu TT, Min D, Succar L, Rangan GK, Hu M, Henderson BR, et al. Disruption of E-cadherin by matrix metalloproteinase directly mediates epithelial-mesenchymal transition downstream of transforming growth factor-beta1 in renal tubular epithelial cells. *Am J Pathol*. 2009;175(2):580–591.
- Inazaki K, Kanamaru Y, Kojima Y, Sueyoshi N, Okumura K, Kaneko K, Yamashiro Y, Ogawa H, Nakao A. Smad3 deficiency attenuates renal fibrosis, inflammation, and apoptosis after unilateral ureteral obstruction. *Kidney Int*. 2004;66(2):597–604.
- Xie P, Sun L, Nayak B, Haruna Y, Liu FY, Kashihara N, Kanwar YS. C/EBP-beta modulates transcription of tubulointerstitial nephritis antigen in obstructive uropathy. *J Am Soc Nephrol*. 2009;20(4):807–819.
- Wang H, Guan Y, Karamercan MA, Ye L, Bhatti T, Becker LB, Baur JA, Sims CA. Resveratrol rescues kidney mitochondrial function following hemorrhagic shock. *Shock*. 2015;44(2):173–180.
- Xu Y, Ruan S, Wu X, Chen H, Zheng K, Fu B. Autophagy and apoptosis in tubular cells following unilateral ureteral obstruction are associated with mitochondrial oxidative stress. *Int J Mol Med*. 2013;31(3):628–636.
- Hyun I. The bioethics of stem cell research and therapy. *J Clin Invest*. 2010;120(1):71–75.
- Takahashi K, Yamanaka S. Induction of pluripotent stem cells from mouse embryonic and adult fibroblast cultures by defined factors. *Cell*. 2006;126(4):663–676.
- Sun D, Bu L, Liu C, Yin Z, Zhou X, Li X, Xiao A. Therapeutic effects of human amniotic fluid-derived stem cells on renal interstitial fibrosis in a murine model of unilateral ureteral obstruction. *PLoS One*. 2013;8(5):e65042.
- Rota C, Imberti B, Pozzobon M, Piccoli M, De Coppi P, Atala A, Gagliardini E, Xinari C, Benedetti V, Fabricio AS, et al. Human amniotic fluid stem cell preconditioning improves their regenerative potential. *Stem Cells Dev*. 2012;21(11):1911–1923.
- Shahrezaie M, Mansour RN, Nazari B, Hassannia H, Hosseini F, Mahboudi H, Eftekhary M, Kehtari M, Veshkini A, Ahmadi Vasmehjani A, et al. Improved stem cell therapy of spinal cord injury using GDNF-overexpressed bone marrow stem cells in a rat model. *Biologicals*. 2017;50:73–80.
- Lin LF, Doherty DH, Lile JD, Bektesh S, Collins F. GDNF: A glial cell line-derived neurotrophic factor for midbrain dopaminergic neurons. *Science*. 1993;260(5111):1130–1132.
- Skaper SD. Neurotrophic factors: An overview. *Methods Mol Biol*. 2018;1727:1–17.
- Cortes D, Carballo-Molina OA, Castellanos-Montiel MJ, Velasco I. The non-survival effects of glial cell line-derived neurotrophic factor on neural cells. *Front Mol Neurosci*. 2017;10:258.
- Pichel JG, Shen L, Sheng HZ, Granholm AC, Drago J, Grinberg A, Lee EJ, Huang SP, Saarma M, Hoffer BJ, et al. Defects in enteric innervation and kidney development in mice lacking GDNF. *Nature*. 1996;382(6586):73–76.
- Sariola H, Saarma M. Novel functions and signalling pathways for GDNF. *J Cell Sci*. 2003;116(Pt 19):3855–3862.
- De Coppi P, Callegari A, Chiavegato A, Gasparotto L, Piccoli M, Taiani J, Pozzobon M, Boldrin L, Okabe M, Cozzi E, et al. Amniotic fluid and bone marrow derived mesenchymal stem cells can be converted to smooth muscle cells in the cryoinjured rat bladder and prevent compensatory hypertrophy of surviving smooth muscle cells. *J Urol*. 2007;177(1):369–376.

24. Hao S, He W, Li Y, Ding H, Hou Y, Nie J, Hou FF, Kahn M, Liu Y. Targeted inhibition of beta-catenin/CBP signaling ameliorates renal interstitial fibrosis. *J Am Soc Nephrol*. 2011;22(9):1642–1653.
25. Lameire N, Jager K, Van Biesen W, de Bacquer D, Vanholder R. Chronic kidney disease: A European perspective. *Kidney Int Suppl*. 2005(99):S30–S38.
26. Costantini F, Shakya R. GDNF/Ret signaling and the development of the kidney. *Bioessays*. 2006;28(2):117–127.
27. Zhang R, Lu Y, Li J, Wang J, Liu C, Gao F, Sun D. Glial cell line-derived neurotrophic factor induced the differentiation of amniotic fluid-derived stem cells into vascular endothelial-like cells in vitro. *J Mol Histol*. 2016;47(1):9–19.
28. Wang J, Wang F, Wang Z, Li S, Chen L, Liu C, Sun D. Protective effect of GDNF-engineered amniotic fluid-derived stem cells on the renal ischaemia reperfusion injury in vitro. *Cell Prolif*. 2018;51(2):e12400.
29. Dendooven A, Ishola DA Jr., Nguyen TQ, Van der Giezen DM, Kok RJ, Goldschmeding R, Joles JA. Oxidative stress in obstructive nephropathy. *Int J Exp Pathol*. 2011;92(3):202–210.
30. Kawada N, Moriyama T, Ando A, Fukunaga M, Miyata T, Kurokawa K, Imai E, Hori M. Increased oxidative stress in mouse kidneys with unilateral ureteral obstruction. *Kidney Int*. 1999;56(3):1004–1013.
31. Holterman CE, Read NC, Kennedy CR. Nox and renal disease. *Clin Sci (Lond)*. 2015;128(8):465–481.
32. Qin J, Xie YY, Huang L, Yuan QJ, Mei WJ, Yuan XN, Hu GY, Cheng GJ, Tao LJ, Peng ZZ. Fluorofenidone inhibits nicotinamide adenine dinucleotide phosphate oxidase via PI3K/Akt pathway in the pathogenesis of renal interstitial fibrosis. *Nephrology (Carlton)*. 2013;18(10):690–699.
33. Qin J, Mei WJ, Xie YY, Huang L, Yuan QJ, Hu GY, Tao LJ, Peng ZZ. Fluorofenidone attenuates oxidative stress and renal fibrosis in obstructive nephropathy via blocking NOX2 (gp91phox) expression and inhibiting ERK/MAPK signaling pathway. *Kidney Blood Press Res*. 2015;40(1):89–99.
34. Kolli VK, Abraham P, Rabi S. Methotrexate-induced nitrosative stress may play a critical role in small intestinal damage in the rat. *Arch Toxicol*. 2008;82(10):763–770.
35. Sun D, Wang Y, Liu C, Zhou X, Li X, Xiao A. Effects of nitric oxide on renal interstitial fibrosis in rats with unilateral ureteral obstruction. *Life Sci*. 2012;90(23-24):900–909.
36. Jiang L, Qiu W, Zhou Y, Wen P, Fang L, Cao H, Zen K, He W, Zhang C, Dai C, et al. A microRNA-30e/mitochondrial uncoupling protein 2 axis mediates TGF-beta1-induced tubular epithelial cell extracellular matrix production and kidney fibrosis. *Kidney Int*. 2013;84(2):285–296.
37. Liu Y. Cellular and molecular mechanisms of renal fibrosis. *Nat Rev Nephrol*. 2011;7(12):684–696.
38. Rocha R, Funder JW. The pathophysiology of aldosterone in the cardiovascular system. *Ann N Y Acad Sci*. 2002;970:89–100.
39. Chen H, Sun F, Zhong X, Shao Y, Yoshimura A, Liu Y. Eplerenone-mediated aldosterone blockade prevents renal fibrosis by reducing renal inflammation, interstitial cell proliferation and oxidative stress. *Kidney Blood Press Res*. 2013;37(6):557–566.
40. Sun GX, Ding R, Li M, Guo Y, Fan LP, Yue LS, Li LY, Zhao M. Ghrelin attenuates renal fibrosis and inflammation of obstructive nephropathy. *J Urol*. 2015;193(6):2107–2115.
41. Sun D, Eirin A, Zhu XY, Zhang X, Crane JA, Woollard JR, Lerman A, Lerman LO. Experimental coronary artery stenosis accelerates kidney damage in renovascular hypertensive swine. *Kidney Int*. 2015;87(4):719–727.
42. Kang DH, Joly AH, Oh SW, Hugo C, Kerjaschki D, Gordon KL, Mazzali M, Jefferson JA, Hughes J, Madsen KM, et al. Impaired angiogenesis in the remnant kidney model: I. Potential role of vascular endothelial growth factor and thrombospondin-1. *J Am Soc Nephrol*. 2001;12(7):1434–1447.
43. Sulikowska B, Rutkowski B, Marszalek A, Maniatis J. The role of interstitial changes in the progression of chronic kidney disease. *Postepy Hig Med Dosw (Online)*. 2015;69:830–837.
44. Campanholle G, Ligresti G, Gharib SA, Duffield JS. Cellular mechanisms of tissue fibrosis. 3. Novel mechanisms of kidney fibrosis. *Am J Physiol Cell Physiol*. 2013;304(7):C591–C603.
45. Otunctemur A, Ozbek E, Cakir SS, Polat EC, Dursun M, Cekmen M, Somay A, Ozbay N. Pomegranate extract attenuates unilateral ureteral obstruction-induced renal damage by reducing oxidative stress. *Urol Ann*. 2015;7(2):166–171.
46. Zhang X, Lemasters JJ. Translocation of iron from lysosomes to mitochondria during ischemia predisposes to injury after reperfusion in rat hepatocytes. *Free Radic Biol Med*. 2013;63:243–253.
47. Brooks C, Wei Q, Feng L, Dong G, Tao Y, Mei L, Xie ZJ, Dong Z. Bak regulates mitochondrial morphology and pathology during apoptosis by interacting with mitofusins. *Proc Natl Acad Sci USA*. 2007;104(28):11649–11654.
48. Bottinger EP, Bitzer M. TGF-beta signaling in renal disease. *J Am Soc Nephrol*. 2002;13(10):2600–2610.
49. Ballermann BJ, Obeidat M. Tipping the balance from angiogenesis to fibrosis in CKD. *Kidney Int Suppl* (2011). 2014;4(1):45–52.
50. Eddy AA, Neilson EG. Chronic kidney disease progression. *J Am Soc Nephrol*. 2006;17(11):2964–2966.